



CHORUS

This is the accepted manuscript made available via CHORUS. The article has been published as:

Design of a Mott Multiferroic from a Nonmagnetic Polar Metal

Danilo Puggioni, Gianluca Giovannetti, Massimo Capone, and James M. Rondinelli
Phys. Rev. Lett. **115**, 087202 — Published 20 August 2015

DOI: [10.1103/PhysRevLett.115.087202](https://doi.org/10.1103/PhysRevLett.115.087202)

Design of a Mott Multiferroic from a Non-Magnetic Polar Metal

Danilo Puggioni,¹ Gianluca Giovannetti,² Massimo Capone,² and James M. Rondinelli¹

¹*Department of Materials Science and Engineering, Northwestern University, IL 60208-3108, USA*

²*CNR-IOM-Democritos National Simulation Centre and International School for Advanced Studies (SISSA), Trieste, Italy*

We examine the electronic properties of newly discovered “ferroelectric metal” LiOsO_3 combining density-functional and dynamical mean-field theories. We show that the material is close to a Mott transition and that electronic correlations can be tuned to engineer a Mott multiferroic state in 1/1 superlattice of LiOsO_3 and LiNbO_3 . We use electronic structure calculations to predict that the $(\text{LiOsO}_3)_1/(\text{LiNbO}_3)_1$ superlattice exhibits strong coupling between magnetic and ferroelectric degrees of freedom with a ferroelectric polarization of $41.2 \mu\text{C cm}^{-2}$, Curie temperature of 927 K, and Néel temperature of 379 K. Our results support a route towards high-temperature multiferroics, *i.e.*, driving non-magnetic *polar metals* into correlated insulating magnetic states.

PACS numbers: 75.85.+t, 71.45.Gm, 77.80.B–, 71.20.–b,

Introduction.—Multiferroics (MF) are a class of insulating materials where two (or more) primary ferroic order parameters, such as a ferroelectric polarization and long-range magnetic order, coexist. Technologically, they offer the possibility to control magnetic polarizations with an electric field for reduced power consumption [1, 2]. Nonetheless, intrinsic room-temperature MF remain largely elusive. This fact may be understood by examining the microscopic origins for the ferroic order: In Type-I MF, ferroelectricity and magnetism arise from different chemical species with ordering temperatures largely independent of one another and weak magnetoelectric (ME) coupling [3]. The ferroelectric ordering also typically appears at temperatures higher than the magnetic order, and the spontaneous polarization P is large since it is driven by a second-order Jahn-Teller distortion, *e.g.*, BiFeO_3 [3, 4]. In Type-II MF, however, magnetic order induces ferroelectricity, which indicates a strong ME coupling between the two order parameters. Nonetheless, P is usually much smaller, *e.g.*, by a factor of 10^2 as in $R\text{-Mn}_2\text{O}_5$ (R being rare earth) [5]. In a few MFs with high-transition temperatures, *i.e.*, BiFeO_3 [6] and $\text{Sr}_{1-x}\text{Ba}_x\text{MnO}_3$ [7–9], magnetism is caused by Mott physics arising from strong correlations. The interactions localize the spins at high temperature, paving the way for magnetic ordering at room temperature. Materials where this robust magnetism is coupled with ferroelectric distortions are ideal candidates for a room-temperature MFs.

Herein, we propose a design strategy for novel Mott MF phases. It relies on tuning the degree of correlation of the recently discovered class of materials referred to as ‘ferroelectric metals’ with LiOsO_3 as the prototypical member [10]. This material is the first undisputed realization of the Anderson-Blount mechanism [11], and challenges the expectation that conduction electrons in metals would screen the electric field induced by polar displacements [10, 12, 13]. Despite robust metallicity, this material shares structural similarities with prototypical *insulating* ferroelectric oxides, such as LiNbO_3 [14, 15]: A $R3c$ crystal structure with acentric cation displacements and distorted OsO_6 octahedra [16, 17] and comparable lattice parameters [10, 14]. While the *polar displacements* in LiNbO_3 rely on cross-gap hybridization between p (O) and d (Nb) states [18], in LiOsO_3 they are weakly coupled to the states at

the Fermi level (E_F), which makes possible the coexistence of an acentric structure and metallicity [16, 19]. In LiOsO_3 the empty d -manifold of LiNbO_3 is replaced by a non-magnetic $5d^3$ ground state with a half-filled t_{2g} (d_{xy} , d_{xz} , d_{yz}) configuration, which is responsible for the metallic response [16]. However, the strength of the electronic interactions is insufficient to drive a Mott transition in the correlated t_{2g} manifold as revealed by low-temperature resistivity measurements; nonetheless, if it would be possible to enhance the electronic correlations in LiOsO_3 and achieve a metal-insulator transition, then a previously unidentified multiferroic material should result. The concept is that if an insulating state can be obtained from a ‘ferroelectric metal’ through enhanced correlations, it would then naturally lead to magnetic ordering of the localized electron spins, coexisting polar displacements.

In this work we explore the feasibility of this approach using a combination of first-principles density functional theory (DFT) plus dynamical mean field theory (DMFT) calculations [20, 21]. We first show that the electronic Coulomb interactions and Hund’s coupling in LiOsO_3 make it an ideal candidate for realizing a Mott MF due to the multi-orbital t_{2g} physics. Next, we describe the design of a new multiferroic by control of the electronic structure through atomic scale engineering of a Mott metal-insulator transition (MIT) in an ultrashort period $(\text{LiOsO}_3)_1/(\text{LiNbO}_3)_1$ superlattice. The insulating and magnetic state is driven by an enhancement of the electronic correlations in LiOsO_3 layers owing to the kinetic energy reduction of the t_{2g} orbitals from the superlattice geometry. The ferroelectric properties mainly originate from cooperative Li and O displacements. The multiferroic phase emerges across the MIT, exhibiting a net electric polarization ($41.2 \mu\text{C cm}^{-2}$) and a G -type antiferromagnetic order [with $0.9 \mu_B$ per Os atom], with calculated magnetic-ordering and ferroelectric temperatures of 379 K and 927 K, respectively. Our results uncover a promising alternative route to discovery of room-temperature multiferroics: One could search for correlated *polar metals near Mott transitions* and drive the phases into insulating states, rather than the often-pursued approach of inducing polar displacements in robustly insulating magnets.

Correlations in LiOsO_3 .—We first examine the effect of the interactions on the metallic state of LiOsO_3 and determine the

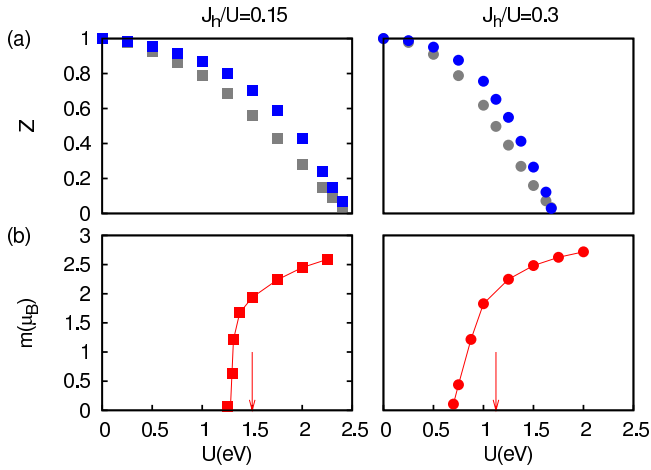


FIG. 1. (Color online) (a) Orbital-resolved quasiparticle orbital weight Z (filled symbols) and (b) local magnetization m (μ_B) (obtained from a spin-polarized calculation) of the t_{2g} orbitals in paramagnetic LiOsO_3 as function of U for different ratios of J_h/U within LDA+DMFT. Vertical arrows indicate the critical value of U required to reach the insulating state in the G -type AFM structure.

critical values for a Mott transition U_c in the paramagnetic and antiferromagnetic (AFM) phases using LDA+DMFT. The criterion for a Mott-Hubbard transition is frequently associated with the ratio between the bandwidth (W) and the interaction strength U , so that the Mott transition occurs for U_c of the order of W . In a multiband Hubbard model with M orbitals, U_c is enhanced by orbital fluctuations, *i.e.*, $U_c \sim \sqrt{MW}$, [29] and it is influenced by the Hund's coupling J_h . Indeed, at half-filling, U_c is *reduced* by an enhancement of J_h [30].

In the following, we show this is precisely the situation in LiOsO_3 [16]. Owing to the energy separation between t_{2g} and e_g orbitals in the density of state of LiOsO_3 about E_F , we resort to using a model for the t_{2g} levels only [16]. Symmetry breaking in bulk LiOsO_3 , also allows the orbitals in the d manifold to mix, which lifts the degeneracy of t_{2g} orbitals with two of states remaining degenerate.

Fig. 1 shows the orbital resolved quasiparticle weight (Z) of the occupied orbitals as a function of U for two different values of J_h/U for paramagnetic LiOsO_3 in the experimental structure (see top panels). Z measures the metallic character of the system, and it evolves from $Z=1$ for a non-interacting metal to $Z=0$ for a Mott insulator. Upon increasing the value of J_h/U , the critical value of U required to reach the Mott state ($Z=0$) is shifted to smaller values of U [30].

In the correlated regime, we anticipate electron localization will lead to long-range magnetic order of the localized spins. Spin-polarized LDA+DMFT calculations, initialized with a G -type AFM structure (every spin on an Os cation is antiparallel to all its neighbors), reveal that the local magnetic moment rapidly saturates to the atomic value $S = 3/2$. The MIT, marked by vertical arrows, occurs for a weaker coupling in the AFM than in the paramagnetic state.

Design of a Mott Multiferroic.—The LDA+DMFT calculations reveal that a simultaneous Mott and magnetic state could

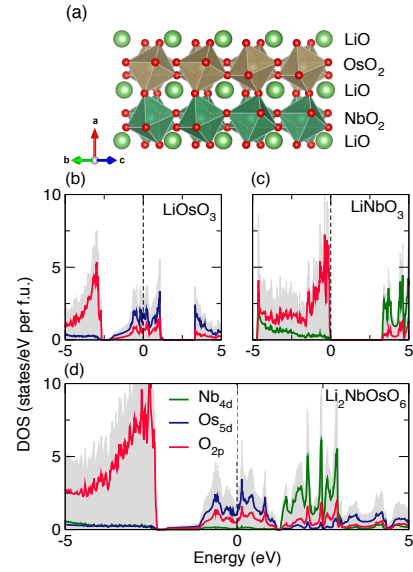


FIG. 2. (Color online) (a) The superlattice exhibits the $a^-b^-b^-$ tilt pattern. Atom- and orbital-resolved DOS for (b) LiOsO_3 , (c) LiNbO_3 and (d) $\text{LiOsO}_3/\text{LiNbO}_3$ at the DFT-LDA level. E_F is given by the (broken) vertical line at 0 eV.

be engineered in LiOsO_3 by reducing the electronic kinetic energy. One avenue to control and decrease the kinetic energy relies on heterostructuring and interleaving two perovskites together to form a coherent superlattice, whereby an isostructural insulator would restrict the electron hopping due to the reduction in available channels [31–33]. Such geometries can be achieved in practice using oxide molecular-beam epitaxy or pulsed-laser deposition methods [34, 35].

Owing to the chemical and structural compatibility of LiOsO_3 with LiNbO_3 , with a lattice mismatch of 3.2%, we devise an ultrashort period perovskite superlattice of $(\text{LiOsO}_3)_1/(\text{LiNbO}_3)_1$ as illustrated in panel (a) of Fig. 2. The superlattice is constructed by beginning from the $R3c$ crystal structure of LiOsO_3 (LiNbO_3) and imposing a layered order along the $[110]$ direction in the rhombohedral setting, which is equivalent to a $1/1$ period superlattice grown along the pseudocubic (pc) $[001]$ direction (see Ref. 21). The geometry in Fig. 2 is also different from a superlattice constructed along the $[101]_{pc}$ direction (see Ref. 36), which is likely more challenging to realize experimentally. Following full relaxation of the superlattice, without any constraints, we find the cation order results in a symmetry reduction to the polar space group Pc with out-of-phase OsO_6 and NbO_6 octahedral rotations, *i.e.*, the $a^-a^-b^-$ tilt pattern given in Glazer notation [37]. The microscopic origin of polar displacements are described below.

Electronic Properties.—Fig. 2 shows the LDA electronic density of states (DOS) for the $\text{LiOsO}_3/\text{LiNbO}_3$ superlattice (d), compared with LiOsO_3 (b) and LiNbO_3 (c) using the LDA-optimized atomic structures. The results for LiOsO_3 (Fig. 2b) highlight the metallic character of the former, where the weight at the Fermi level (E_F) mainly comes from Os $5d$ states which show strong admixture from the O $2p$ states. In

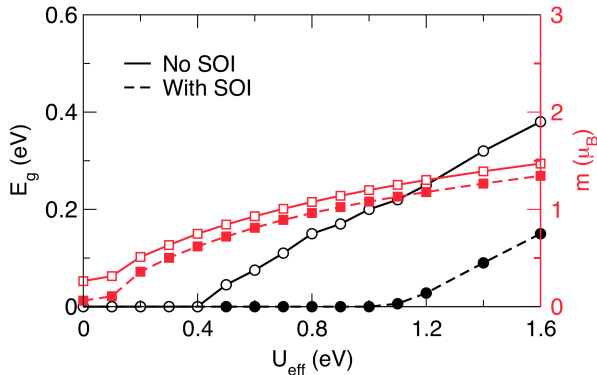


FIG. 3. (Color online) Band gap E_g and averaged local magnetic moment for Os as a function of U_{eff} with and without spin-orbit interaction (SOI) for the $\text{LiOsO}_3/\text{LiNbO}_3$ superlattice.

contrast, LiNbO_3 is a band insulator, with the O $2p$ states forming the valence band and Nb $4d$ states at the conduction band minimum, separated by a gap of 3.28 eV (Fig. 2c). In the superlattice, we find essentially no charge transfer between Os and Nb: Each component (LiOsO_3 and LiNbO_3) is isoelectronic to its bulk configuration; the DOS can be described as a direct superposition of the two components (Fig. 2d). The Os $5d$ states partially fill the gap in the electronic spectrum formed from the two-dimensional NbO_2 planes. There is some spectral weight transfer in the vicinity of E_F among the Os orbitals, which are sensitive to the electron correlation strength as shown in Fig. 1.

We now explore the effect of electronic correlations by means of LSDA+ U calculations at different values of $U_{\text{eff}} = U - J_h$. An accurate value of the Hubbard U is unknown for perovskite osmates, but it is expected to be comparable to that of NaOsO_3 [40] and double perovskite $\text{Sr}_2\text{CrOsO}_6$ [41] for which a correct description of the electronic properties are obtained with U values of 1.0 and 2.0 eV, respectively. Note that the differences from various implementations of the LDA+ U scheme for bulk LiOsO_3 were found to be minor [16], and are anticipated to also be insignificant for the superlattice.

Fig. 3 shows the evolution in the band gap (E_g) and magnetic moment of Os^{3+} ions (m) as a function of U_{eff} for LSDA including spin-orbit interaction (SOI, broken lines). A gap opens at a critical $U_{\text{eff}} \sim 1$ eV (U_c), signaling a MIT into a magnetic insulating ground state. As expected the $\text{LiOsO}_3/\text{LiNbO}_3$ superlattice becomes an G -type antiferromagnetic insulator for smaller values of the interaction with respect to bulk LiOsO_3 .

The reduction in U_c for the MIT in the superlattice can be understood by analyzing the effect of the geometrical confinement on the t_{2g} band dispersions. (For simplicity, we use the LDA electronic structures given in Ref. 21.) While the bandwidth of the d_{xy} orbitals is essentially the same as for bulk LiOsO_3 , the d_{xz} and d_{yz} bands in $\text{LiOsO}_3/\text{LiNbO}_3$ are significantly narrowed as a consequence of the reduced hop-

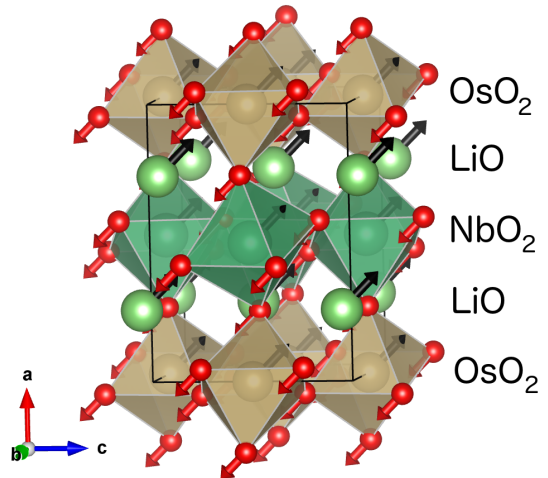


FIG. 4. (Color online) Illustration of the polar zone-center mode along the $[101]$ -direction labeled by irrep Γ_2^- . Anti-polar displacements along the $[010]$ -direction are omitted for clarity.

ping along the superlattice direction. This leads to a reduction of the kinetic energy which enhances the electron-electron correlations thus favoring electron localization. The nearly localized electrons behave as almost localized spins and give rise to AFM ordering which drives a MIT already at moderate interaction strengths (Fig. 3 and 4 in Ref. 21). The crucial role of AFM in driving the system insulating, which in turn makes the system ferroelectric, can be interpreted as a sign of strong interaction between the local magnetic moment and the ferroelectric order of the superlattice.

We note that when SOI are excluded in the calculations (Fig. 3, solid lines), the MIT occurs at a further reduced correlation strength ($U_c \sim 0.5$ eV), and the magnetic moment only slightly increases. Such behaviors are also observed in bulk LiOsO_3 [16]. At values below U_c , the superlattice is weakly ferrimagnetic before the G -AFM transition.

As in $\text{SrTiO}_3/\text{SrRuO}_3$ [38, 39], the ordering of the B -site lattice is fundamental to achieving the MIT in the superlattice. For example, in the case of random occupancy of the B -site by Os and Nb atoms, the superlattice would likely behave as a metal because there would be no confinement imposed by the “blocking” niobate layers on a local scale. However, we anticipate that the large ionic size mismatch (11%) between Nb^{5+} and Os^{5+} should provide a driving force for ordering during growth.

Ferroelectric Polarization.—We now apply a group theoretical analysis [42, 43] of the $\text{LiOsO}_3/\text{LiNbO}_3$ structure to understand the inversion symmetry-breaking displacements that produce the Pc ground state. We use a fictitious $P2_1/c$ centrosymmetric phase (where polar displacements are switched off) as the reference phase from which the symmetry-adapted mode displacements are obtained as different irreducible representations (irreps) of the $P2_1/c$ space group operators [44]. We find the loss of inversion symmetry mainly derives from cooperative Li and O displacements in the (010) mirror plane

of the Pc phase. Moreover, we find anti-polar displacements along the b -axis which result in no net polarization. All polar displacements are described by a distortion vector that corresponds to the irrep Γ_2^- along the [101]-direction of the Pc structure (Fig. 4). These displacements are consistent with the acentric Li and O ionic displacements identified to be responsible for lifting inversion symmetry in bulk LiOsO_3 [10, 13] and across the ferroelectric transition in LiNbO_3 [45].

We now compute the ferroelectric polarization in $\text{LiOsO}_3/\text{LiNbO}_3$ using the Berry's phase approach [46] within $\text{LSDA}+U$ ($U_c = 0.5$ eV). The spontaneous electric polarization of the Pc phase is $32.3 \mu\text{C cm}^{-2}$ and $25.5 \mu\text{C cm}^{-2}$ along the [100]-direction, *i.e.*, along the pseudo-cubic [001] superlattice repeat direction and [001]-directions, respectively. (Note that the [101]-direction in $\text{LiOsO}_3/\text{LiNbO}_3$ corresponds to the polar [111]-direction in LiNbO_3 .) Together this yields a net polarization along the [101]-direction of $41.2 \mu\text{C cm}^{-2}$. These values are also robust to SOI, with a change of less than 15% in P . Recently, it was suggested that the Curie temperature (T_C) can be calculated from the energy difference between the high- and low-symmetry phases, leading to an interpretation as the thermal energy for the Curie point [47]. To check this approach, we first estimated the T_C for LiNbO_3 by calculating the energy difference between the non-polar $R3c$ and polar $R3c$ phases. We found a critical temperature of 1489 K, which is in excellent agreement with the experimental value ($T_C=1415$ K) [48], indicating the reliability of this scheme for the superlattice. Following the same approach, we use the energy difference between the $P2_1/c$ and Pc structures to obtain a ferroelectric Curie temperature of 927 K for the superlattice. This value is close to the transition temperature for LiNbO_3 (1489 K) [48], and it far exceeds that of bulk LiOsO_3 where inversion symmetry is lost near 140 K [10].

Magnetic Ordering Temperature.—Our DMFT calculations indicate that when the superlattice material enters in the Mott state the magnetic moment is $\sim 3 \mu_B$, corresponding to a high-spin $S = 3/2$ state. We now estimate the Néel temperature for $\text{LiOsO}_3/\text{LiNbO}_3$ by extracting the exchange interaction constants from spin-polarized DFT energies computed at U_c without SOI following the approach in Ref. 49. We calculate the total energy for G -type, A -type, C -type AFM, and ferromagnetic order. Assuming that the magnetism arises by ordering localized spins, we obtain intra- and inter-plane Os–Os exchange magnetic couplings of -5.6 meV and -0.2 meV respectively, where a negative interaction indicates G -type AFM exchange. From these values we estimate a Néel temperature of 671 K for the superlattice. We also apply Anderson's renormalization [50] which reduces the magnetic ordering temperature to 379 K and suggests that the superlattice is a correlation-induced room-temperature multiferroic. We also examined the effect of epitaxial strain on the critical temperatures of the superlattice by clamping the in-plane lattice parameters of the equilibrium $(\text{LiOsO}_3)_1/(\text{LiNbO}_3)_1$ structure to be those of LaAlO_3 (3.794 \AA , placing the superlattice under tensile strain), a common perovskite substrate. We then relaxed the out-of-plane lattice parameter until the stresses along this direction were

within the relaxation tolerance. Here we find that $T_C=1532$ K and $T_N=282$ K, where T_N is renormalized as described in the main text. Although the T_C increases, the T_N decreases. The T_N is close to the room temperature, therefore, we propose that using YAlO_3 (3.692 \AA) or SrLaAlO_3 (3.757 \AA) as substrate would act to increase T_N . Note that the same renormalization has been used successfully for comparisons of the calculated Néel temperatures of BiFeO_3 , $R\text{TcO}_3$ ($R = \text{rare earth}$), BiCrO_3 and NaOsO_3 with the experimental values [51–55].

Conclusions.—We used a $\text{LDA}+\text{DMFT}$ approach to study the electronic properties of the polar metal LiOsO_3 . A detailed understanding of the electronic structure shows that a reduction of the kinetic energy can drive the system into a Mott insulating state. We use this concept to propose a strategy to design multiferroic materials by constructing a superlattice with the uncorrelated polar dielectric LiNbO_3 . On the basis of $\text{LSDA}+U$ calculations, we show that the ultra-short period $\text{LiOsO}_3/\text{LiNbO}_3$ superlattice should be a room-temperature Mott multiferroic with a large $41.2 \mu\text{C cm}^{-2}$ electric polarization. Note that the ordering and ratio between LiOsO_3 and LiNbO_3 layers in the superlattice is crucial to achieve the multiferroic state, as the artificial phase relies on the susceptibility of LiOsO_3 to become insulating. The general expectation is that in a $(\text{LiOsO}_3)_n/(\text{LiNbO}_3)_m$ superlattice, the MIT should persist only with $m \geq n = 1$. In fact, this is the configuration where the LiNbO_3 “blocking” layers can optimally reduce the bandwidth of LiOsO_3 layer. We also note that a similar dimensional control of electronic phase transitions is well-established in nickelates and ruthenates [56, 57].

The large ferroelectric displacements from the LiNbO_3 layers facilitate the high ferroelectric ordering temperature in the $\text{LiOsO}_3/\text{LiNbO}_3$ heterostructure as observed from the similarity in the Curie temperature of the superlattice with that of LiNbO_3 . In this case, $\text{LiOsO}_3/\text{LiNbO}_3$ would behave as a paramagnetic Mott ferroelectric at high temperatures and transition into Mott multiferroic below the Néel temperature, which is predicted to be well-above room temperature. We hope this work motivates the synthesis of new artificial multiferroics, and the adds to the growing discussion of new applications where noncentrosymmetric metals and ferroelectric materials may be united.

GG and MC acknowledge financial support by the European Research Council under FP7/ERC Starting Independent Research Grant “SUPERBAD” (Grant Agreement No. 240524). DP and JMR acknowledge the ARO under Grant Nos. W911NF-12-1-0133 and W911NF-15-1-0017 for financial support and the DOD-HPCMP for computational resources.

-
- [1] T. Kimura et al. , Nature (London) **426**, 55 (2003).
 - [2] N. Hur et al. , Nature (London) **429**, 392 (2004).
 - [3] J. Wang et al. , Science **299**, 1719 (2003).
 - [4] R. G. Pearson, Journal of Molecular Structure: THEOCHEM **103**, 25 (1983).
 - [5] S.-W. Cheong and M. Mostovoy, Nat. Mat. **6**, 13 (2007).

- [6] Sanghyun Lee, M. T. Fernandez-Diaz, H. Kimura, Y. Noda, D. T. Adroja, Seongsu Lee, Junghwan Park, V. Kiryukhin, S.-W. Cheong, M. Mostovoy, and Je-Geun Park Phys. Rev. B **88**, 060103(R) (2013)
- [7] H. Sakai, J. Fujioka, T. Fukuda, D. Okuyama, D. Hashizume, F. Kagawa, H. Nakao, Y. Murakami, T. Arima, A. Q. R. Baron, Y. Taguchi, and Y. Tokura, Phys. Rev. Lett. **107**, 137601 (2011)
- [8] G. Giovannetti, S. Kumar, C. Ortix, M. Capone, and J. van den Brink, Phys. Rev. Lett. **109**, 107601 (2012).
- [9] R. Nourafkan, G. Kotliar, and A.-M. S. Tremblay, Phys. Rev. B **90**, 220405(R) (2014)
- [10] Y. Shi, Y. Guo, X. Wang, A. J. Princep, D. Khalyavin, P. Manuel, Y. Michiue, A. Sato, K. Tsuda, S. Yu, M. Arai, Y. Shirako, M. Akaogi, N. Wang, K. Yamaura and A. T. Boothroyd, Nat. Mat. **12**, 1024 (2013).
- [11] P. W. Anderson and E. I. Blount, Phys. Rev. Lett. **14**, 217 (1965).
- [12] Q. Yao, H. Wu, K. Deng, and E. Kan, RSC Adv. **4**, 26843 (2014)
- [13] Sim Hyunsu and Kim Bog G., Phys. Rev. B **89** 201107 (2014).
- [14] H. Boysen and F. Altorfer, Acta Crystallogr. B **50**, 405 (1994).
- [15] H.D. Megaw, Acta Crystallogr. Section A **24**, 583 (1968).
- [16] G. Giovannetti and M. Capone, Phys. Rev. B **90**, 195113 (2014)
- [17] H. Sim and B. G. Kim, Phys. Rev. B **89**, 201107(R) (2014).
- [18] I. Inbar and R. E. Cohen, Phys. Rev. B **53**, 1193 (1996).
- [19] D. Puggioni and J. M. Rondinelli, Nat. Commun. **5**, 3432 (2014).
- [20] A. Georges, G. Kotliar, W. Krauth, and M. J. Rozenberg, Rev. Mod. Phys. **68**, 13 (1996).
- [21] See Supplemental Material at [URL will be inserted by publisher] which includes Refs. [22–28] for calculation details, discussion of the superlattice construction, equilibrium atomic positions using the LDA and LSDA+ U with $U = 0.5$ eV, and additional electronic structures. Note for simplicity, we assume $\alpha = \beta = \gamma = 90^\circ$ which slightly shifts the results by few percent, but the constraint is anticipated to be appropriate for coherent epitaxial growth.
- [22] G. Kresse and J. Furthmuller, Phys. Rev. B **54**, 11 169 (1996); Comput. Mater. Sci. **6**, 15 (1996).
- [23] M. Capone, L. de’ Medici, and A. Georges, Phys. Rev. B **76**, 245116 (2007).
- [24] P. E. Blöchl, Phys. Rev. B **50**, 17953 (1994).
- [25] H. J. Monkhorst and J. D. Pack, Phys. Rev. B **13**, 5188 (1976).
- [26] R. B. Lehoucq, D. C. Sorensen, and C. Yang, ARPACK Users’ Guide (SIAM, Philadelphia, 1997).
- [27] H. T. Stokes and D. M. Hatch, “FINDSYM: Program for Identifying the Space Group Symmetry of a Crystal.” J. Appl. Cryst. **38**, 237-238 (2005), ISOTROPY Software Suite, iso.byu.edu,.
- [28] A. A. Mostofi, J. R. Yates, Y.-S. Lee, I. Souza, D. Vanderbilt and N. Marzari, Comput. Phys. Commun. **178**, 685 (2008).
- [29] O. Gunnarsson, E. Koch, and R. Martin, Phys. Rev. B **54** R11026 (1996)
- [30] A. Georges, L. de’ Medici, J. Mravlje, Annual Reviews of Condensed Matter Physics **4**, 137-178 (2013).
- [31] B. Gray, H.N. Lee Ho, J. Liu, J. Chakhalian, and J.W. Freeland, Appl. Phys. Lett. **97** 013105 (2010).
- [32] S. Middey, D. Meyers, M. Kareev, E. J. Moon, B. A. Gray, X. Liu, J. W. Freeland, and J. Chakhalian, Appl. Phys. Lett. **101** 261602 (2012).
- [33] S. Middey, P. Rivero, D. Meyers, M. Kareev, X. Liu, Y. Cao, J.W. Freeland, S. Barraza-Lopez, and J. Chakhalian, Sci. Rep **4** 6819 (2014).
- [34] D. G. Schlom, L.-Q. Chen, X. Pan, A. Schmehl, and M.A. Zurbuchen, J. Amer. Ceram. Soc. **91** 2429 (2008).
- [35] Blok J. L., Wan X., Koster, G., Blank D. H. A. and Rijnders G., Appl. Phys. Lett. **99** 151917 (2011).
- [36] H. J. Xiang, Phys. Rev. B **90**, 094108 (2014).
- [37] A. M. Glazer, Acta Cryst. A **31**, 756 (1975)
- [38] Mingqiang Gu, Qiyun Xie, Xuan Shen, Rubin Xie, Jianli Wang, Gang Tang, Di Wu, G. P. Zhang, and X. S. Wu, Phys. Rev. Lett. **109**, 157003 (2012).
- [39] S.L. Cuffini, V.A. Macagno, R.E. Carbonio, A. Melo, E. Trolund, J.L. Gautier, J. Sol. State Chem. **105**, 161 (1993).
- [40] Y. G. Shi, Y. F. Guo, S. Yu, M. Arai, A. A. Belik, A. Sato, K. Yamaura, E. Takayama-Muromachi, H. F. Tian, H. X. Yang, J. Q. Li, T. Varga, J. F. Mitchell, and S. Okamoto, Phys. Rev. B **80**, 161104(R) (2009).
- [41] O. Nganba Meetei, Onur Erten, Mohit Randeria, Nandini Trivedi, and Patrick Woodward, Phys. Rev. Lett. **110**, 087203 (2013).
- [42] D. Orobengoa, C. Capillas, M. I. Aroyo, and J. M. Perez-Mato, Journal of Applied Crystallography **42**, 820 (2009).
- [43] J. M. Perez-Mato, D. Orobengoa, and M. I. Aroyo, Acta Cryst. A **66**, 558 (2010).
- [44] The ferroelectric transition in LiOsO_3 and LiNbO_3 is $R\bar{3}c \rightarrow R3c$. Using the same method described in the main paper for the construction of the superlattice but starting from the $R\bar{3}c$ crystal structure of LiOsO_3 (LiNbO_3) the atomic relaxation of the ‘idealized’ superlattice gives the centrosymmetric $P21/c$ phase. This structure is used as the reference for both the mode decomposition and in the calculation of the ferroelectric Curie temperature.
- [45] N. A. Benedek, and C. J. Fennie, The Journal of Physical Chemistry C **117** 13339 (2013)
- [46] R.D. King-Smith and D. Vanderbilt, Phys. Rev. B **47**, 1651 (1993); D. Vanderbilt and R. D. Smith, Phys. Rev. B **48**, 4442 (1993).
- [47] Jacek C. Wojdel and Jorge Íñiguez, arXiv:1312.0960.
- [48] Palatnikov, M.N. and Sidorov, N.V. and Skiba, V.I. and Makarov, D.V. and Biryukova, I.V. and Serebryakov, Yu.A. and Kravchenko, O.E. and Balabanov, Yu.I. and Kalinnikov, V.T., Inorganic Materials **36**, 489 (2000).
- [49] N. Lampis, C. Franchini, G. Satta, A. Geddo-Lehmann, and S. Massidda, Phys. Rev. B **69**, 064412 (2004).
- [50] P. W. Anderson, Phys. Rev. **115**, 2 (1959).
- [51] P. Baettig, C. Ederer, and N. A. Spaldin, Phys. Rev. B **72**, 214105 (2005).
- [52] C. Franchini, T. Archer, Jiangang He, Xing-Qiu Chen, A. Filipetti, and S. Sanvito, Phys. Rev. B **83**, 220402(R) (2011).
- [53] V. S. Borisov, I. V. Maznichenko, D. B’ttcher, S. Ostanin, A. Ernst, J. Henk, and I. Mertig, Phys. Rev. B **85**, 134410 (2012).
- [54] Y. Xu, X. Hao, J. Meng, D. Zhou and F. Gao, J. Phys: Condens. Matter **21**, 236006 (2009).
- [55] S. Middey, Saikat Debnath, Priya Mahadevan, and D. D. Sarma, Phys. Rev. B **89**, 134416 (2014).
- [56] Boris, A. V. and Matiks, Y. and Benckiser, E. and Frano, A. and Popovich, P. and Hinkov, V. and Wochner, P. and Castro-Colin, M. and Detemple, E. and Malik, V. K. and Bernhard, C. and Prokscha, T. and Suter, A. and Salman, Z. and Morenzoni, E. and Cristiani, G. and Habermeier, H.-U. and Keimer, B., Science **332**, 937 (2011).
- [57] Freeland, J. W. and Chakhalian, J. and Boris, A. V. and Tonnerre, J.-M. and Kavich, J. J. and Yordanov, P. and Grenier, S. and Zschack, P. and Karapetrova, E. and Popovich, P. and Lee, H. N. and Keimer, B., Phys. Rev. B **81**, 094414 (2010).